

Supporting Information for

Desorption Trends of Small Alcohols and the Disruption of Intermolecular Interactions at Defect Sites on Au(111)

Eric M. Maxwell^a, Lyssa A. Garber^a, Clayton J. Rogers^a, Ava J. Galgano^a, Jordon S. Baker^{a,b},
Hasan Kaleem^a, David T. Boyle^{a,c}, Jessica L. Berry^a, and Ashleigh E. Baber^{*a}

^aDepartment of Chemistry and Biochemistry, James Madison University, Harrisonburg, VA
22807

^bDepartment of Chemistry, Virginia Commonwealth University, Richmond, VA 23284

^cDepartment of Chemistry, Stanford University, Stanford, CA 94305

High coverages of methanol (Fig S1), ethanol (Fig S2), 1-propanol (Fig S3), 1-butanol (Fig S4), 2-butanol (Fig S5), and isobutanol (Fig S6) were studied using UHV-TPD. For each alcohol studied, the desorption features corresponding to the surface layer (kinks, step edges, and terraces) populated prior to the filling of multilayer peaks. Alcohol multilayer desorption features had lower desorption temperatures and energies compared to the surface features for each alcohol.

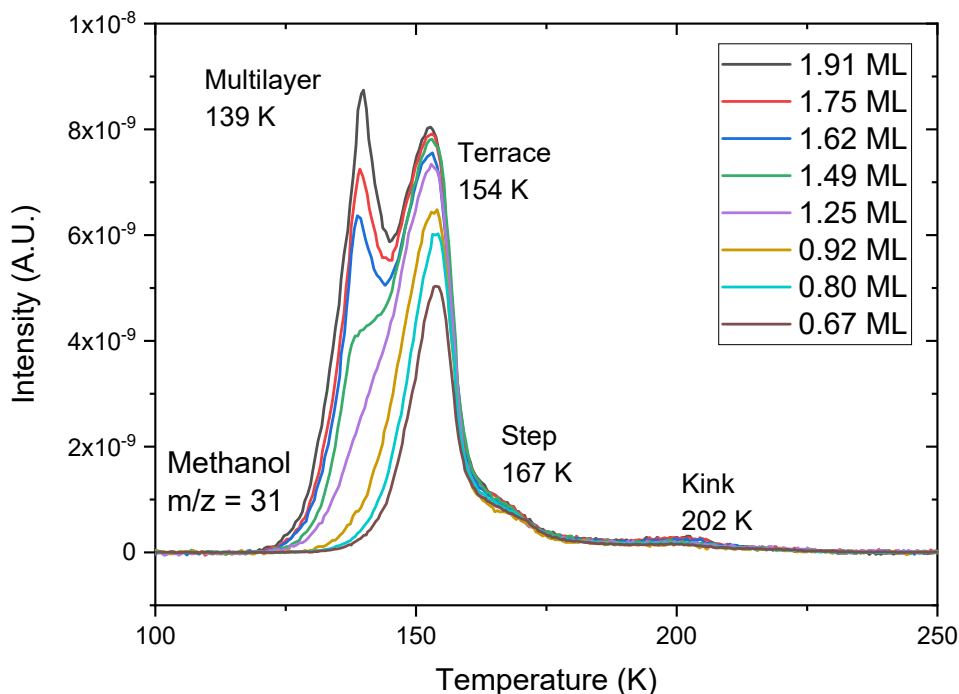


Figure S1. High coverage TPD study of methanol desorption ($m/z = 31$) from Au(111). (heating rate = 1.19 ± 0.03 K/s)

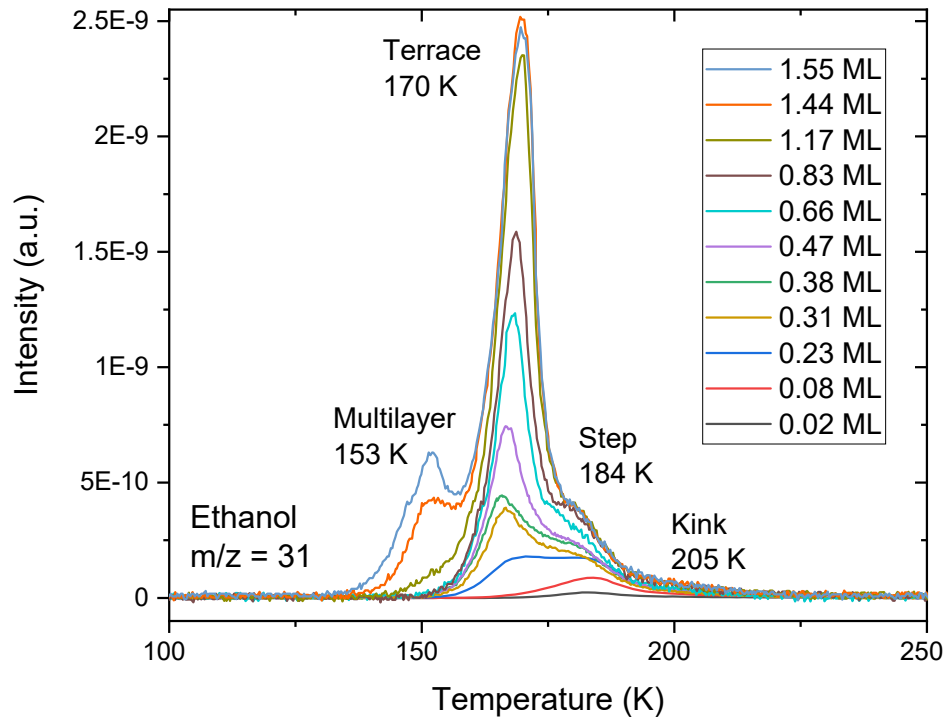


Figure S2. TPD coverage study of ethanol desorption ($m/z = 31$) from Au(111). (heating rate = 1.19 ± 0.03 K/s)

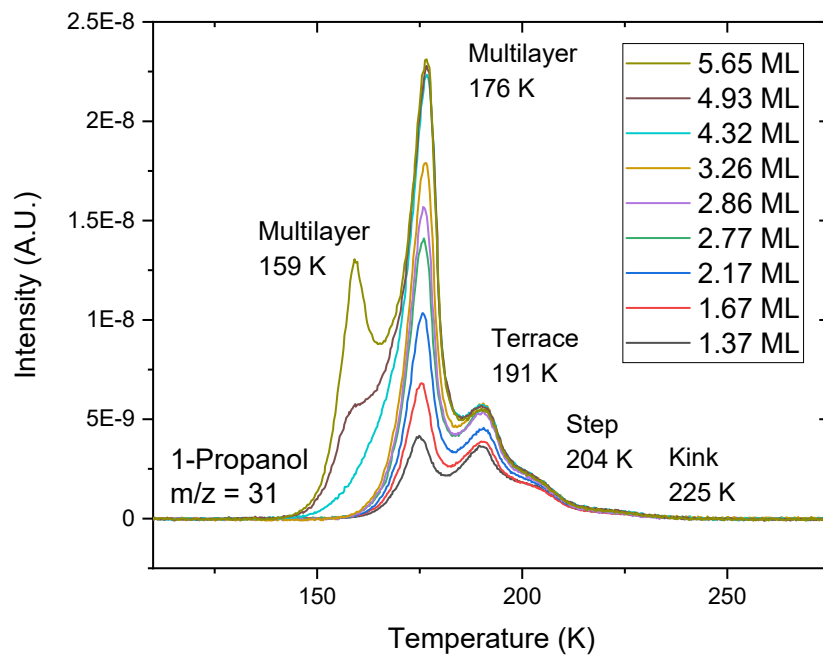


Figure S3. High coverage TPD study of 1-propanol desorption ($m/z = 31$) from Au(111). (heating rate = 0.96 ± 0.04 K/s)

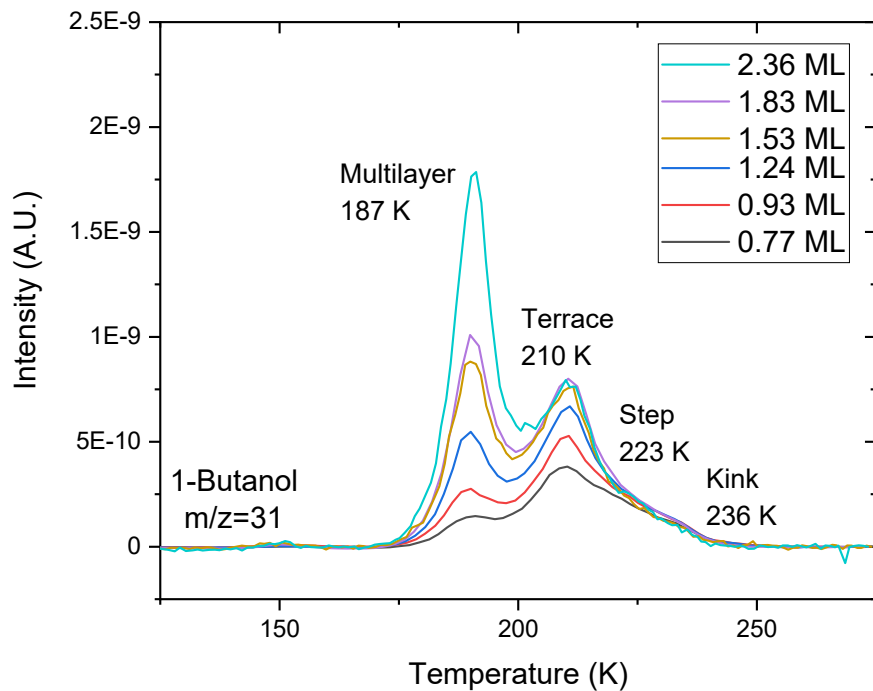


Figure S4. High coverage TPD study of 1-butanol desorption ($m/z = 31$) from Au(111). (heating rate = 0.94 ± 0.03 K/s)

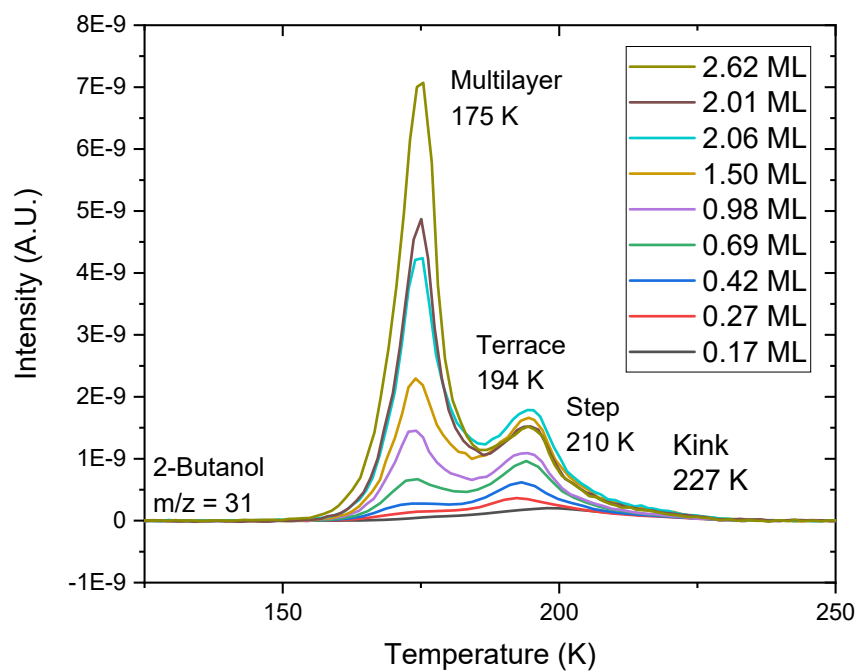


Figure S5. High coverage TPD study of 2-butanol desorption ($m/z = 31$) from Au(111). (heating rate = 1.52 ± 0.05 K/s)

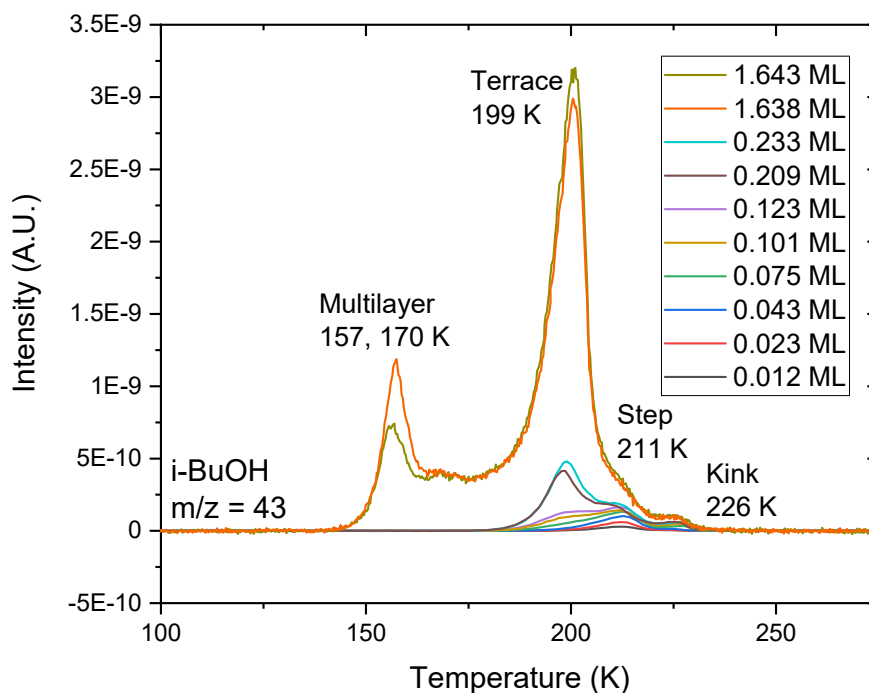


Figure S6. High coverage TPD study of isobutanol desorption ($m/z = 43$) from Au(111). (heating rate = 0.81 ± 0.03 K/s)

Table S1. Desorption energies and errors (kJ/mol) for all small alcohols studied on Au(111) terrace, step edge, and kink sites. Desorption energies were calculated using the first order Redhead approximation and prefactors of 10^{12} . Errors are reported for the terrace desorption site for each alcohol studied: experimental error for terrace desorption features of ± 5 K; inherent error in the Redhead analysis of 1.5% when using $10^{13} \geq \nu/\beta \geq 10^8$; and error based on the difference in an order of magnitude for the assumed prefactors when calculating desorption energies.

	terrace (kJ/mol)	step (kJ/mol)	kink (kJ/mol)	errors for terrace desorption site (kJ/mol)		
				experimental (± 5 K)	Redhead analysis ($\pm 1.5\%$)	prefactor assumption ($\pm 10^1$)
MeOH	37.2	40.4	49.2	± 1.2	± 0.56	± 2.95
EtOH	41.9	45.1	52.7	± 1.3	± 0.63	± 3.29
PrOH	47.7	50.2	56.9	± 1.3	± 0.72	± 3.71
1-BuOH	51.5	54.8	58.1	± 1.3	± 0.77	± 4.02
2-BuOH	46.8	50.8	56.0	± 1.2	± 0.70	± 3.71
isoBuOH	49.1	52.2	56.0	± 1.3	± 0.74	± 3.81

In the following figures, S7 – S12, TPD plots of a representative (A) alcohol desorbing from Au(111) are compared to (B) fragmentation data, where the alcohol was dosed into the chamber and directly monitored using mass spectrometry. For the control data, a flat background was obtained prior to

dosing the alcohol of interest into the chamber at two distinct pressures prior to closing the leak valve and waiting for a return to the baseline. The mass spec settings were the same for the TPD and control fragmentation measurements. All data were corrected for the quadrupole's relative sensitivity setting prior to background subtraction in Origin Pro. The comparison of small alcohol TPD and control fragmentation patterns demonstrates that the small alcohols do not dissociate on Au(111). Rather, small alcohol adsorb and desorb molecularly from Au(111).

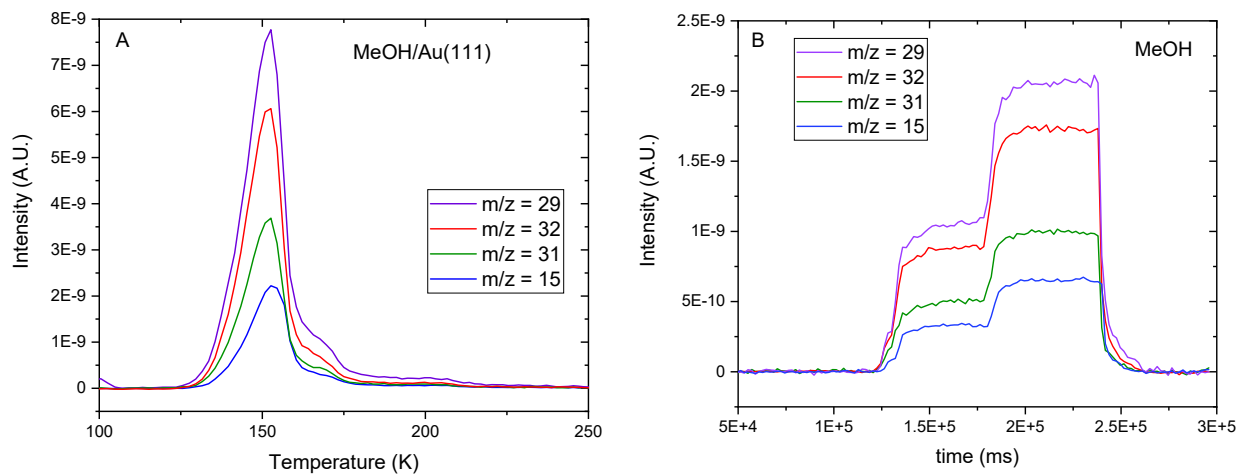


Figure S7. MeOH A) TPD from Au(111) and B) control measurements. The control MeOH fragmentation patterns were collected by monitoring $m/z = 29, 32, 31,$ and 15 while dosing MeOH into the chamber. The P_{MeOH} was increased to 4.2×10^{-8} torr and then 8.5×10^{-8} torr before closing the leak valve and allowing the pressure to return to baseline.

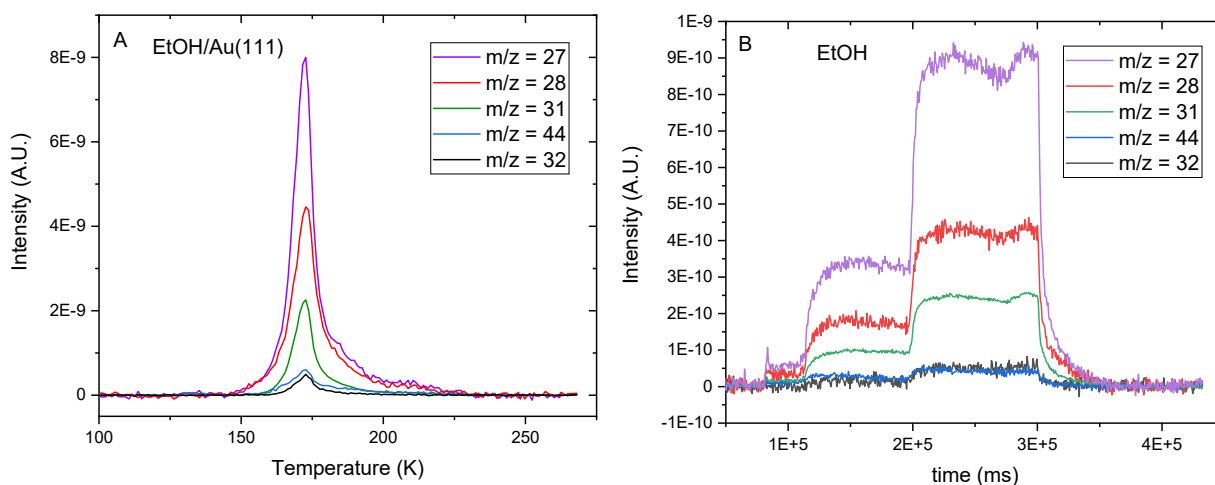


Figure S8. EtOH A) TPD from Au(111) and B) control measurements. The control EtOH fragmentation patterns were collected by monitoring $m/z = 27, 28, 31, 44,$ and 32 while dosing EtOH into the chamber. The P_{EtOH} was increased to 3.4×10^{-8} torr and then 8.5×10^{-8} torr before closing the leak valve and allowing the pressure to return to baseline.

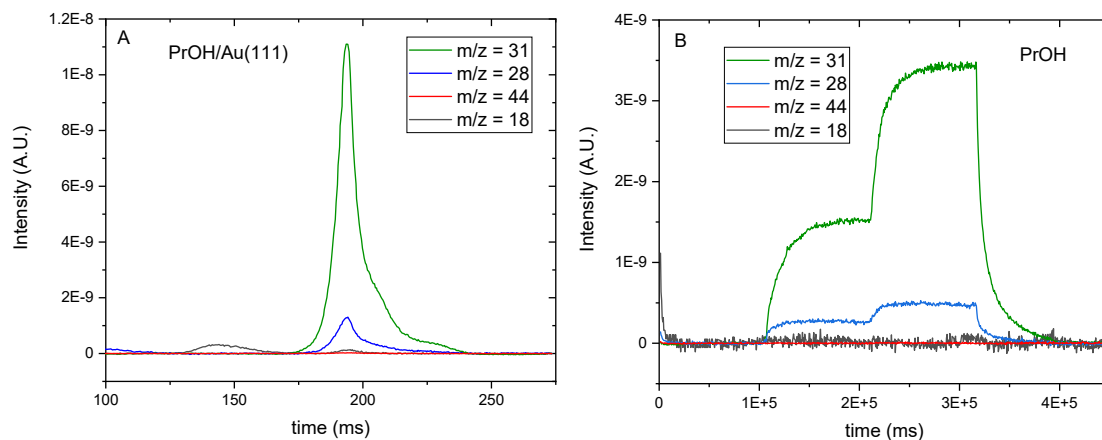


Figure S9. PrOH A) TPD from Au(111) and B) control measurements. The control PrOH fragmentation patterns were collected by monitoring $m/z = 31, 28, 44,$ and 18 while dosing PrOH into the chamber. The P_{PrOH} was increased to 3.6×10^{-8} torr and then 7.0×10^{-8} torr before closing the leak valve and allowing the pressure to return to baseline.

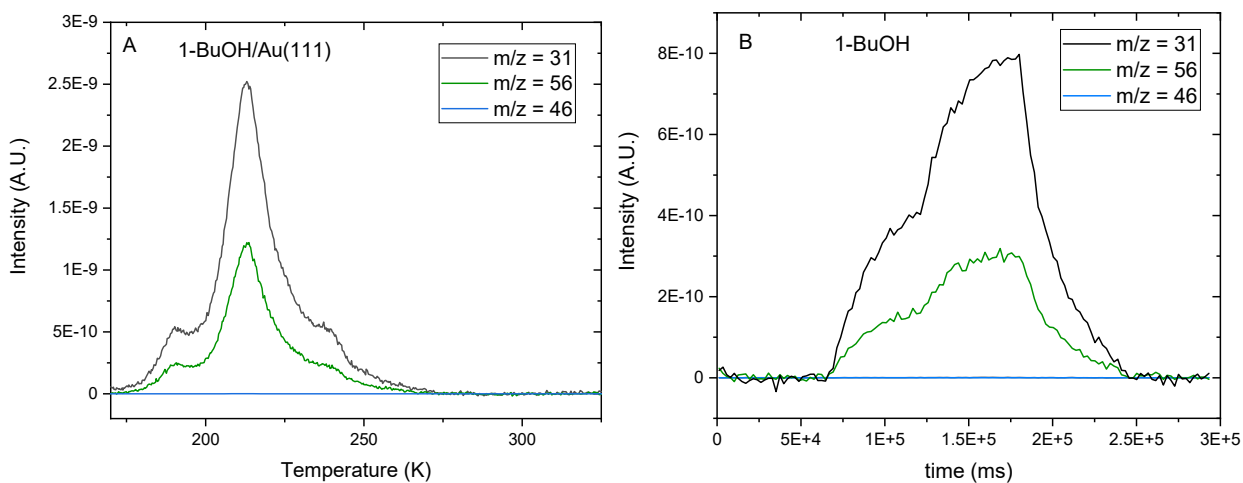


Figure S10. 1-BuOH A) TPD from Au(111) and B) control measurements. The control 1-BuOH fragmentation patterns were collected by monitoring $m/z = 31, 28, 44,$ and 18 while dosing 1-BuOH into the chamber. The $P_{\text{1-BuOH}}$ was increased to 6.2×10^{-8} torr and then 8.5×10^{-8} torr before closing the leak valve and allowing the pressure to return to baseline.

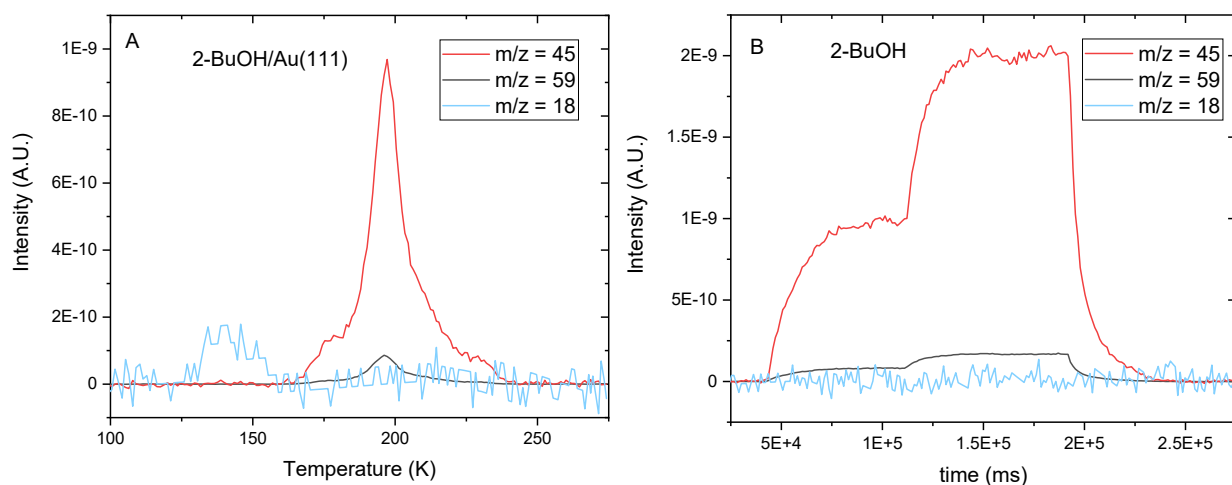


Figure S11. 2-BuOH A) TPD from Au(111) and B) control measurements. The control 2-BuOH fragmentation patterns were collected by monitoring $m/z = 31, 28, 44,$ and 18 while dosing 2-BuOH into the chamber. The $P_{2\text{-BuOH}}$ was increased to 5.0×10^{-8} torr and then 9.2×10^{-8} torr before closing the leak valve and allowing the pressure to return to baseline.

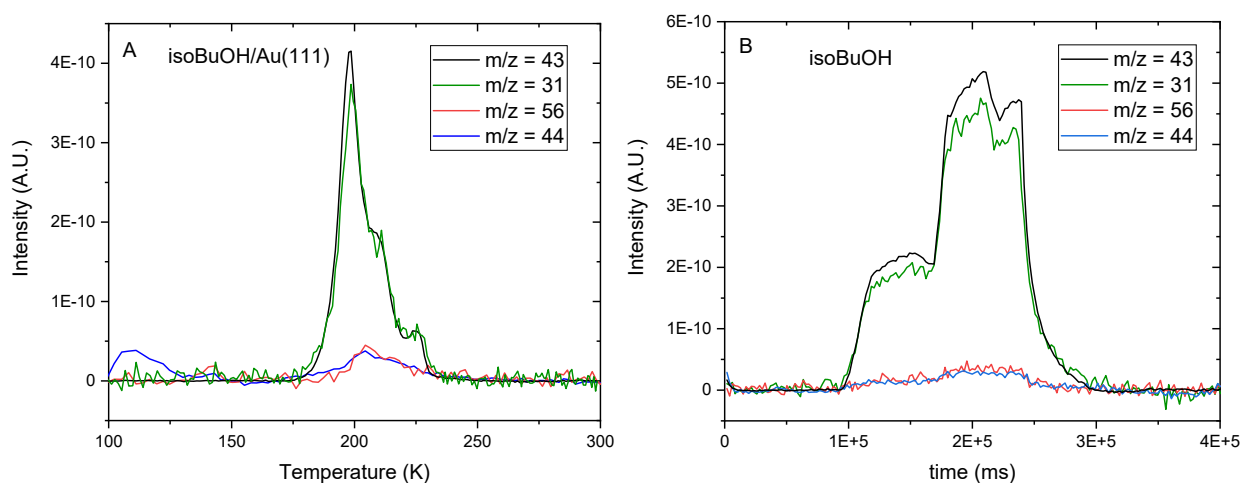


Figure S12. IsoBuOH A) TPD from Au(111) and B) control measurements. The control isoBuOH fragmentation patterns were collected by monitoring $m/z = 31, 28, 44,$ and 18 while dosing isoBuOH into the chamber. The P_{isoBuOH} was increased to 3.0×10^{-8} torr and then 6.4×10^{-8} torr before closing the leak valve and allowing the pressure to return to baseline.